Adjacent Effect on Positive Charge Transfer from Radical Cation of *n*-Dodecane to Scavenger Studied by Picosecond Pulse Radiolysis, Statistical Model, and Monte Carlo Simulation

Akinori Saeki,* Takahiro Kozawa, Yoichi Yoshida, and Seiichi Tagawa*

The Institute of Scientific and Industrial Research, Osaka University, 8-1 Mihogaoka, Ibaraki, Osaka 567-0047, Japan

Received: August 10, 2003; In Final Form: December 12, 2003

Time-dependent behavior of radical cation in *n*-dodecane in the presence of cation scavenger at high concentration was measured by picosecond pulse radiolysis. The initial yields decreased with the increase of scavenger concentrations ranging from 0.05 to 4 M. This reduction could not be explained by a first-order rate constant. To solve this discrepancy, we propose an adjacent effect of solute molecules and examined it by a statistical model and Monte Carlo simulation. The relationship with the static quenching model in the photolysis was also discussed. The calculation results showed good agreement with the experimental data.

1. Introduction

Low LET radiation such as high energy electron beam causes ionization and excitation in material. The ionization gives rise to radical cations and electrons with excess energy. The electrons with sufficient energy cause further ionization and excitation until they lose their energies and become thermalized. In an early stage of a physical reaction, intermediate species such as a radical cation and a thermalized electron exist in a spur which is produced along the trajectory of the incident and secondary electrons. The pair of the parent radical cation and the thermalized electron is called a geminate ion pair.

In a nonpolar liquid, most of the geminate ion pairs recombine through the diffusion in the Coulombic field, since the Coulomb force between the ions can reach a long distance due to the low dielectric constant. This reaction is called a geminate ion recombination.[1] Considerable effort has been devoted to understanding this reaction both experimentally[2−15] and theoretically.[16−24]

Stroboscopic pulse radiolysis is one of the promising methods to measure such a fast reaction and has been developed all over the world.[25−34] Previously, the measurement of reactions that occur within 30 ps had been difficult because of a low time resolution for a few decades. Therefore, in the case of diffusion-controlled reaction, the direct observation of scavenging phenomena had been carried out only in dilute solutions because these reaction are basically too fast to detect. As for a laser flash photolysis, these reactions in the presence of high concentration scavenger have not been reported yet due to experimentally difficulties. On the other hand, since radiation can ionize molecules randomly, one can perform experiments in high concentrated solutions using the pulse radiolysis technique. Several years ago, the time resolution of our system was enhanced with the help of magnetic pulse compression[31] and time jitter compensation techniques.[32] In addition, an effective way to improve the accuracy of the data was invented and applied to picosecond pulse radiolyses.[34] It allows us to carry out experiments with about 10 times better S/N ratio than the previous one.

In this paper, we focus on the scavenging reaction at high solute concentration using the picosecond pulse radiolysis. This reaction not only attracts scientific interest but also is important in that there are many multicomponent industrial materials such as resist material. This work is expected to be useful for understanding the reaction mechanism at high concentration.

2. Experimental Section

The experiments were carried out by means of the subpicosecond pulse radiolysis system utilizing a stroboscopic method which is called pump and probe spectroscopy in the photolysis. A pulsed high energy electron beam from L-band linac (27 MeV)[31] and fundamental oscillation of a femtosecond Ti:sapphire laser (790 nm) were used as an irradiation source and an analyzing light, respectively. The timing between the electron pulse and the laser pulse was changed by an optical delay which were placed in the optical path of the analyzing light. Even though these pulses are synchronized via a common radio frequency (81 MHz), a time jitter of several picoseconds still remains. To reduce the degradation of the time resolution, a time jitter compensation system was utilized.[32] The light detection is based on a double laser pulse technique to enhance the S/N ratio.[34]

A liquid *n*-dodecane was used as a solvent. The use of *n*-dodecane is due to the fact that the absorption peak of its radical cation is near the fundamental oscillation of the Ti:sapphire laser, and the absorption coefficient is larger than other *n*-alkanes at this wavelength.[7] Triethylamine (TEA) was employed as a cation scavenger because it reacts with the radical cation, and its dielectric constant (2.42) is relatively close to the one of *n*-dodecane (2.01). The samples were prepared at TEA concentration from 0.05 to 4 M and deaerated by Ar gas bubbling to eliminate the remaining O_2 gas. The experiments were carried out at room temperature. The time-dependent behaviors of pure *n*-dodecane and TEA were also measured for the reference of the absorption intensity. Each decay includes

* Corresponding authors. E-mail: saeki03@sanken.osaka-u.ac.jp, tagawa@sanken.osaka-u.ac.jp; Tel: +81-6-6879-8502; Fax: +81-6-6876-3287.

10.1021/jp036372m CCC: $27.50
Published on Web 02/10/2004

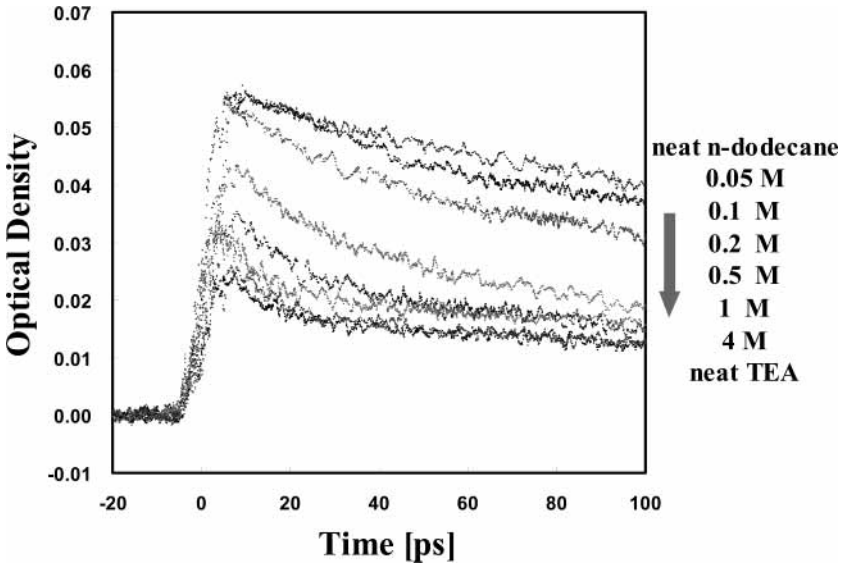

Figure 1. Time-dependent behavior of radical cation at 790 nm in *n*-dodecane in the presence of TEA.

about 3700 points and was smoothed by moving the average for every 10 points.

3. Result and Discussion

The time-dependent behaviors of radical cations in pure solvent and solute−solvent system are shown in Figure 1. Typical decays of the geminate ion recombination in neat *n*-dodecane and the one in the presence of TEA are also shown. The initial optical densities of the radical cation were smaller than the expected values derived from first-order kinetics, especially at high concentrations. If the scavenging reaction by TEA follows first-order kinetics, the initial value should be closer to the one of the neat *n*-dodecane. Even if a time-dependent rate constant[19] was applied to the experimental data, the discrepancy still remained. In a case of a low time resolution measurement, the reduction of initial yield is observed due to the convolution of raw data. However, the time resolution in this paper is enough high to discuss the initial yield. As for the contribution of excited state of *n*-dodecane,[7] the time profiles monitored at 805[11,28]and 1300 nm,[11] the latter of which is ascribed to absorption of electron, were measured in the past and showed good correspondence to each other. Furthermore, since the excited state forms primarily from the geminate ion recombination, its contribution to the initial yield is thought to be negligible. In a polar liquid such as water, the presolvated electron, which is a precursor of solvated electron and has a high mobility, reacts with anion scavenger such as acetone,[35−37] so the initial yield of solvated electron decreases, while the one in a concentrated perchloric acid solution does not.[38] Besides, Czapski and Peled[39] mentioned the direct formation of an encounter pair in water with high concentrated anion scavenger. As for a precursor of solvent radical cation,[1,40] we have not had any evidence to deny its existence. A preliminary calculation including a contribution of high mobile precursor was carried out and showed correspondence with the experimental data with a parameter set regarding a precursor with a lifetime of 10 ps and a mobility of 50 times larger than that of a normal radical cation. However, other sets of parameters are thought to show the correspondence as well. In addition, the ratio of absorption coefficients at monitored wavelength should be considered when a complete assignment is needed. Namely, there are several uncertain parameters when a precursor of a radical cation is introduced. On the other hand, to take an adjacent effect (vide infra) into account is natural at high concentration. Therefore, we focused on this phenomenon in this work. The first-order rate constant between a radical cation of *n*-dodecane and TEA was estimated to be $(0.5-1.0) \times 10^{10}$ M^{-1} s^{-1} from several low concentrated solutions up to 1 ns. This value is compatible with the one expected from diffusion. Therefore, the contribution of a high mobility ion[41−47] does not have to be considered in *n*-alkane, as mentioned previously.[41]

The reaction rate is mainly determined by the diffusion and activation energy including collision frequency and steric factor. Since the hole transfer from radical cation of *n*-alkane to TEA is diffusion-controlled,[1,9] these species react within one collision. Therefore, if these reactants are adjacent to another when the ionization takes place, they do not need to diffuse to react. We assumed the cause of the initial significant reduction to be a phenomenon that a solvent molecule is adjacent to several TEA molecules at high concentration. Under such a condition, the radical cation of the solvent will be spontaneously scavenged by the adjacent TEA molecules within the time resolution of the measurement system. The contribution of multiion pair (or multispur)[24] on the time profile of radical cation may exist, but it does not affect the comparison of normalized initial yield of radical cation in neat and solute-added solution.

To examine this adjacent effect and quantify the reduction of initial yield, we attempted statistical and Monte Carlo approaches.

Statistical Model. Let us define $N_{solvent}$ and n_{solute} as the total number of solvent and solute molecules in an unit volume, respectively. These values are calculated using the density ρ g/cm^3 and molecular weight M of the solvent and the solute concentration c. In addition to these values, the difference of the excluded volume between solute and solvent molecules must be taken into account. The a, a ratio of excluded volume of TEA to that of *n*-dodecane in the actual solute−solvent system, was estimated experimentally to be 0.63.[48] This value is close to 0.61 obtained by using ρ and M. Thus, the relationship between $N_{solvent}$ and n_{solute} is given by eq 1 using $a = 0.63$.

$$\frac{n_{solute}}{N_{solvent}} = c\left(\frac{1000\rho}{M} - ca\right)^{-1} \quad (1)$$

Not only solvent molecules are surrounding solute molecule, but also the solute molecules themselves are thought to

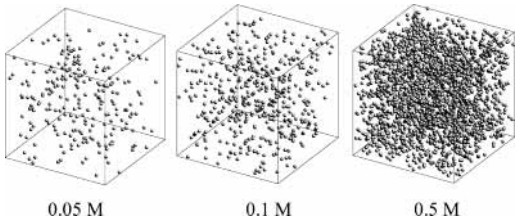

Figure 2. Images of solute distribution obtained by a random insertion.

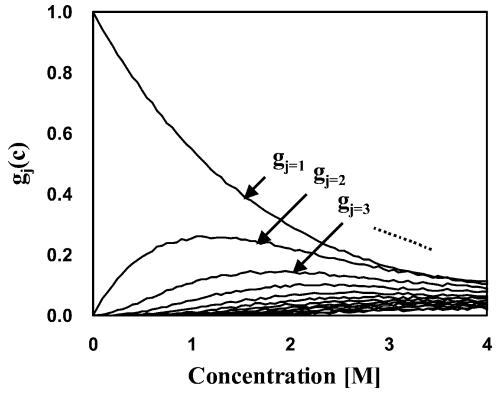

Figure 3. Distribution of the aggregating solute. The *j* means a cluster which consists of *j* solute molecules. If the center of each solute is less than 0.61 nm, they are treated as a cluster.

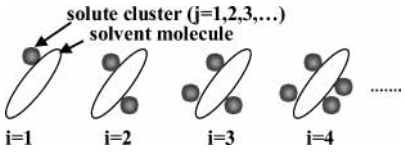

Figure 4. Illustration of the adjacent solute and solvent molecules.

aggregate. Therefore, we estimated the aggregation of solute molecules with the help of the Monte Carlo method. In this calculation, we assumed for simplicity that a solute molecule has a spherical shape and does not have any chemical and physical interactions between them. The solute molecules were randomly inserted into a box. Images of solute distribution were illustrated in Figure 2. The box is a 20 nm cube, corresponding 240 solute molecules at 0.05 M concentration. Actually in the calculation, to prevent the degradation of the calculation accuracy which occurs especially at low concentration (= small number of molecules), the number of solute molecules was fixed at 1000 over the whole concentration with changing the box size. Assuming that the solute molecules are regarded as a cluster if the distance between their center is less than a certain length *d*, the distribution of the solute random aggregation was constructed. The calculations of the distribution were performed 50 times and averaged, resulting in less than 0.5% deviation. Figure 3 shows the result using $d = 0.6$ nm. The *j* represents a cluster which consists of *j* solute molecules, e.g., $j = 1$ is equal to one isolated solute molecule, while $j = 2, 3, ...$ are clusters. The vertical axis represents probability of a cluster denoted as $g_j(c)$ for *j*th cluster. The summation of $g_j(c)$ over *j* at a certain concentration *c* is equal to 1 ($\sum g_j(c) = 1$). The value of $g_1(c)$ decreased with an increase in concentration. On the other hand, the contribution of other clusters had a peak value.

Next, we proceed to formulate the adjacent effect. At high concentration, one solvent molecule may be adjacent to several solute clusters as shown in Figure 4. We assumed that the radical cation is scavenged if at least one solute clusters is adjacent to a solvent molecule because this reaction is diffusion-controlled.[1,9] Therefore, the probability of a solvent molecule adjacent to *i* solute clusters is in the following binomial form using the combinational function $n_{\text{cluster}}C_i$

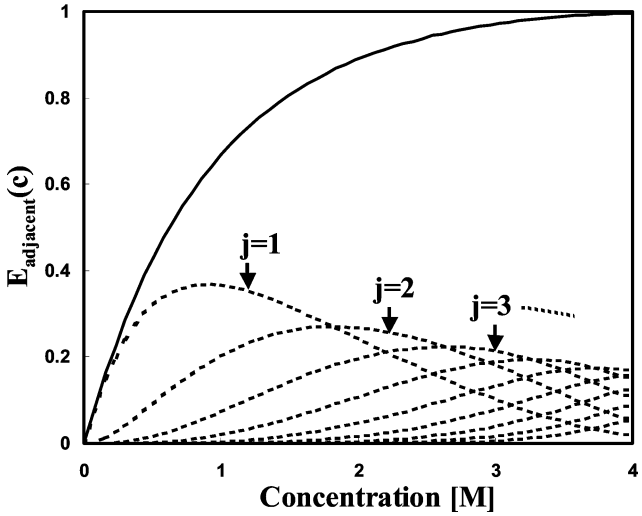

Figure 5. Adjacent effect of the solvent molecules obtained by eqs 1, 3, and 4 and the result of Figure 3. The dotted and solid lines represent the contribution of the *j*th cluster and the sum of the contributions, respectively.

$$n_{\text{cluster}}C_i\left(\sum_{j=1}^{j_{\max}}\frac{g_j(c)}{j}\frac{b_j(c)}{N_{\text{solvent}}}\right)^i\left(1-\sum_{j=1}^{j_{\max}}\frac{g_j(c)}{j}\frac{b_j(c)}{N_{\text{solvent}}}\right)^{n_{\text{cluster}}-i} \tag{2}$$

where $b_j(c)$, n_{cluster}, and $j_{\max}$ are the average number of solvent molecules which are adjacent to *j*th solute cluster, a total number of solute clusters, and a maximum number of *j*, respectively. The $j_{\max}$ was obtained in the calculation to be up to around 30 that was obtained from the calculation in Figure 3. However, as seen in Figure 3, the contributions of large *j* are negligibly small. In this statistical model, the effect of the molecule's shape, conformation, and interaction among molecules are not considered explicitly. The n_{cluster} is given by eq 3 using *j*, $j_{\max}$, $g_j(c)$, and n_{solute}.

$$n_{\text{cluster}} = \sum_{j=1}^{j_{\max}}\frac{g_j(c)}{j}n_{\text{solute}} \tag{3}$$

Since the adjacent events of $i = 1, 2, ..., i_{\max}$ are independent, the total adjacent effect must be summed by *i* from 1 to $i_{\max}$ ($=j_{\max}$).

$$E_{\text{adjacent}}(c) = \sum_{i=1}^{i_{\max}} n_{\text{cluster}}C_i\left(\sum_{j=1}^{j_{\max}}\frac{g_j(c)}{j}\frac{b_j(c)}{N_{\text{solvent}}}\right)^i\left(1-\sum_{j=1}^{j_{\max}}\frac{g_j(c)}{j}\frac{b_j(c)}{N_{\text{solvent}}}\right)^{n_{\text{cluster}}-i} \tag{4}$$

By using eqs 1, 3, and 4, the adjacent effect was calculated with a fitting parameter of $b_j(c)$ and illustrated in Figure 5. The dotted and solid lines represent the contribution of *j*th cluster and the sum of the contributions, respectively. As seen in Figure 5, the contributions of large solute cluster are small, meaning that there are many fitting parameters (b_1, b_2, ..., $b_{j_{\max}}$), but dominant parameters are from b_1 to around b_4. At low concentration, b_1 and b_2 are main fitting parameters. With the increase of concentration, b_3 and b_4 begin to affect the adjacent

TABLE 1: Comparison of Experimental Data to Analytical Value

concn	exptl[a]	$E_{excluded}$[b]	$E_{adajacent}$[c]	calcd[d]
neat	1	0	0	1
0.05 M	1.00	0.007	0.033	0.98
0.1 M	0.97	0.014	0.107	0.93
0.2 M	0.80	0.028	0.199	0.87
0.5 M	0.69	0.071	0.428	0.73
1.0 M	0.58	0.142	0.668	0.59
4.0 M	0.45	0.567	0.997	0.43
neat TEA	0.43	1.000	1.000	0.43

[a] Initial value of the optical density which was normalized by neat *n*-dodecane value. The error was about 0.08 for each value. [b] Excluded effect obtained by eq 8. [c] Adjacent effect obtained by eqs 1, 3, and 4 and the result of Figure 3. [d] Calculated value obtained by eq 9.

effect. Besides, these values used in the calculation (b_1, b_2, b_3, b_4, ...) = (5, 7, 9, 10, ...) are reasonable as listed in Table 2.

If one want to obtain only the $E_{adjacent}$ without the contributions of *j*th cluster, eq 4 can be reduced to eq 5 by subtracting the probability of nonadjacent probability ($i = 0$) from 1. In this form, i_{max} disappears.

$$E_{adjacent}(c) = 1 - \left(1 - \sum_{j=1}^{j_{max}} \frac{g_j(c)}{j} \frac{b_j(c)}{N_{solvent}}\right)^{n_{cluster}} \quad (5)$$

By applying the Poisson theorem and substituting eq 5 for eqs 1 and 3, eq 5 is reduced to the following static quenching formula:

$$\lim_{n_{cluster} \to \infty} E_{adjacent}(c) = 1 - e^{-cV(c)} \quad (6)$$

$$V(c) = \left(\frac{1000\rho}{M} - ca\right)^{-1} \left(\sum_{j=1}^{\infty} \frac{g_j(c)}{j}\right) \left(\sum_{j=1}^{\infty} \frac{g_j(c)\, b_j(c)}{j}\right) \quad (7)$$

In the conventional static quenching model,[49-51] a parameter *V* is the static quenching constant. On the other hand, in our model, *V* is not constant anymore and described as a function of solute concentration. The meaning of *V* in the static quenching model has been interpreted by the "transient effect model",[52] the "sphere of action model",[49] and the "dark complex model".[53] In the transient effect model, the *V* comes from an approximation of time-dependent rate constant according to Weller.[52] However, as mentioned in this paper, the time-dependent rate constant could not reproduce the experimental data. The second and third models are related with each other. The sphere of action model is based on the situation that a quencher molecules happens to be within a sphere of action whose volume is denoted as $V/N_A = 4\pi r^3/3$, where N_A and *r* are Avogadro's number and a radius of the sphere. The relationship of this model with ours will be discussed in the next subsection. The dark complex model suggests the excitation of encounter complex of solute and quencher. This model is the closest to our model among these three models, though the *V* in our model is a function of *c* and expressed by the following three important parameters: (i) $g_j(c)$, the distribution function of solute cluster which reflects the degree of solute aggregation and/or association; (ii) $b_j(c)$, the average number of solvent molecules adjacent to *j*th solute cluster, which implicitly includes the conformational effect on the reaction; and (iii) *a*, the ratio of excluded volume of solute to that of solvent molecule.

In addition to the adjacent effect, we have to take into account the effect that a large part of the solvent molecules is excluded by the solute molecules especially at high concentration. This effect can be analytically described by eq 8.

$$E_{excluded}(c) = \frac{Mca}{1000\rho} \quad (8)$$

The optical absorption of TEA radical cation was reported to lie in the UV region.[54] Since this absorption is strong and broad, the tail of the absorption was observed at 790 nm. Therefore, when we compare the calculation results with the experimental data, the overlap of TEA radical cation should be involved. The ratio of its absorption to that of *n*-dodecane radical cation was 0.43 obtained from Figure 1. The optical density (OD) for comparison which includes $E_{adjacent}$, $E_{excluded}$, and the absorption overlap of TEA and *n*-dodecane radical cations is represented by eq 9.

$$OD = (1 - E_{excluded})(1 - E_{adjacent}) + 0.43(1 - E_{excluded})E_{adjacent} + 0.43E_{excluded} \quad (9)$$

Table 1 shows the comparison of calculated values with the experimental ones. These values showed a good agreement, suggesting that a large part of solvent molecules are adjacent to several solute molecules at high concentration. Therefore, the significant reduction of initial yield was explained by $E_{excluded}$ and $E_{adjacent}$.

Monte Carlo Configurational-Bias Simulation. The effect of the molecule's shape, conformation, and interaction among molecules is not considered explicitly in the statistical model. To take these effects into account, we reproduced the solute−solvent system by using Monte Carlo simulation. The configurational-bias Monte Carlo technique has been developed to insert a chain molecule into a condensed matter.[55-57] This method has been also applied to a vapor−liquid phase and indicated a good agreement with experimental data.[58] Thus, we adopted this method to reproduce the liquid system and examine the adjacent effect in this work. This method divides the potential energy of an atom into two portions: (1) the internal energy u^{int}, which means the intramolecular interactions such as torsion, and (2) the external energy u^{ext}, which includes the intermolecular interactions between the atom and atoms of other molecules.

The OPLS (optimized potentials for liquid simulations) model of Jorgensen et al.[59] was used as a potential energy model. This model was refined by Hautman and Klein[60] to take the bond-bending energy into consideration. The OPLS model treats CH_2 and CH_3 groups as united atoms. The Lennard-Jones potential between *i* united atom and *j* united atom, which are r_{ij} apart from each other, is described by

$$u^{LJ}(r_{ij}) = 4\epsilon_{ij}\left[\left(\frac{\sigma_{ij}}{r_{ij}}\right)^{12} - \left(\frac{\sigma_{ij}}{r_{ij}}\right)^{6}\right] \quad (10)$$

Here, a parameter set of $\epsilon_{CH_2} = 59.4$ K, $\epsilon_{CH_3} = 88.1$ K, $\epsilon_N = 85.9$ K, $\sigma_{CH_2,\ CH_3} = 0.35$ nm, and $\sigma_N = 0.33$ nm was used.[58,61] The ϵ_{ij} and σ_{ij} were calculated according to the mixing rule[62] of $\epsilon_{ij} = \sqrt{\epsilon_i \epsilon_j}$ and $\sigma_{ij} = \sqrt{\sigma_i \sigma_j}$. The Coulomb potential should be included into the external energy potential.

$$u^{Coulomb}(r_{ij}) = \frac{q_i q_j e^2}{4\pi\epsilon_r \epsilon_0 r_{ij} k_B} \quad (11)$$

The variables of $q_N = -0.63$, $q_{CH_2,CH_3\ in\ amine} = 0.105$, and $q_{CH_2,CH_3\ in\ alkane} = 0$ were used.[61] The external energy u^{ext} is the sum of u^{LJ} and $u^{Coulomb}$ which are integrated over other molecules.

The intramolecular energy includes bond bending and torsion energies. For the bond bending energy u^{bend}, the van der Ploeg and Berendsen potential[63] was used

$$u^{\text{bend}}(\theta) = \frac{1}{2}k_\theta(\theta - \theta_0)^2 \tag{12}$$

where $k_\theta = 6.25 \times 10^4$ K rad^{-2} and equilibrium angle of C−C−C bond $\theta_0 = 112.7°$. The angle of C−N−C bond was taken as 107.2°.[61] For the torsion potential, the original Ryckaert and Bellemans potential[64] was used.

$$u^{\text{tors}}(\phi) = \sum_{k=0}^{5} c_k \cos^k(\phi) \tag{13}$$

with dihedral angle ϕ. The coefficients c_k were $c_0 = 1116$ K, $c_1 = 1462$ K, $c_2 = -1578$ K, $c_3 = -368$ K, $c_4 = 3156$ K, and $c_5 = -3788$ K.[64] The vibrational energy was ignored, so that C−C and C−N bond lengths were taken as a constant value 0.153[58]and 0.145 nm,[61] respectively. The internal energy u^{int} is the sum of u^{bend} and u^{tors}.

A chain molecule is grown up atom by atom. First, an initial atom is inserted at a random position. However, this simple random insertion sometimes causes an overlap with another molecule. Therefore, assuming that the united atom is a spherical shape with a radius of 0.15 nm, the random insertion is repeated until the overlap of these united atoms does not take place. This random insertion is not valid in the case of polar solution such as water, showing water molecule clustering due to its strong hydrogen bond. On the other hand, dielectric constants of TEA and *n*-dodecane are almost the same as described above; the random insertion and resulting random clustering are not thought to differ from the real system very much. Second, to insert the next atom *l*, the *k* orientations are generated. The *k* orientations are denoted by a set of vector $\{\mathbf{b}\}_k = \mathbf{b}_1, \mathbf{b}_2, ..., \mathbf{b}_k$ and generated randomly according to the following probability

$$p_l^{\text{int}}(\mathbf{b}_i) = \frac{\exp[-u_l^{\text{int}}(\mathbf{b}_i)/T]}{\sum_i \exp[-u_l^{\text{int}}(\mathbf{b}_i)/T]} \tag{14}$$

where T is absolute temperature and was taken as room temperature. In our calculations, 15 orientations $\mathbf{b}_1$, $\mathbf{b}_2$, ..., $\mathbf{b}_{15}$ were selected from 1000 orientations, which were generated with 10 divided θ ranging from $\theta_0 - 2°$ to $\theta_0 + 2°$ and with 100 divided ϕ ranging from 0° to 360°.

Finally, out of these *k* orientations, one orientation is selected according to eq 15.

$$p_l^{\text{ext}}(\mathbf{b}_i) = \frac{\exp[-u_l^{\text{ext}}(\mathbf{b}_i)/T]}{\sum_i \exp[-u_l^{\text{ext}}(\mathbf{b}_i)/T]} \tag{15}$$

These calculations are continued until the last atom of the molecule is placed. After the configuration of the molecule is fixed, the next molecule is generated following the same procedure. Selection of the next molecule was also done randomly according to the corresponding concentration. Sometimes, we confront a situation that there is no way to avoid an overlap with other molecules. In that case, we canceled the growth of present molecule and calculate it again from the insertion of a first atom, so that we were able to obtain an appropriate configuration of molecules without any overlap.

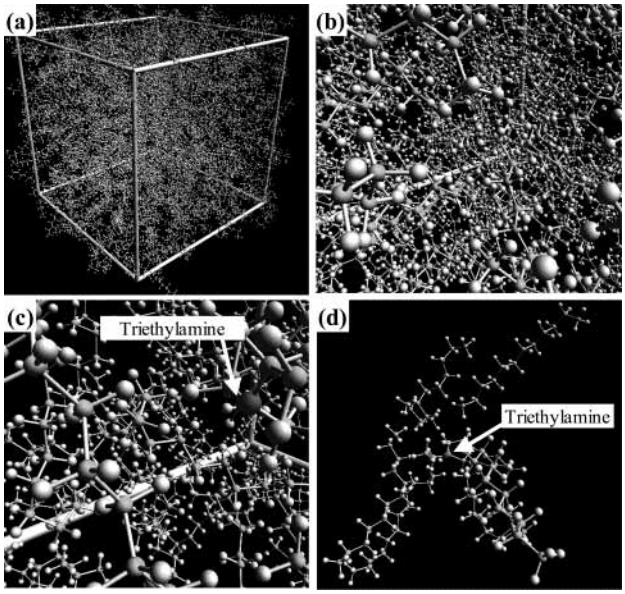

Figure 6. Snapshots of the configurational-bias Monte Carlo simulation. (a) Overview of the box where the solute and solvent molecules were inserted. (b, c) The view inside the box. The radius of the atoms are depicted smaller than the real radius. (d) Extracted several solvent molecules neighbored by a solute molecule.

Figure 6 shows the snapshot of configurational-bias Monte Carlo simulation producing the TEA−*n*-dodecane system. Figure 6a is an overview of a box where the molecules were inserted. The positions of hydrogen atoms were automatically determined from the positions of a carbon and its dihedral angle. Throughout the calculations, the number of the solvent molecules was 500. Therefore, the number of solute molecules and the volume of the box were changed according to each concentration. The calculation was performed one time, resulting in 5.5% deviation.

The adjacent effect was calculated in the inner region that is smaller than the box depicted in Figure 6a because the insertion of molecules was not completed in the peripheral area. Therefore, we narrowed the inner region for calculating the adjacent effect until the density of that region reaches a reasonable value. This narrowing is due to that there is free space in the peripheral area. In this area, the density, which is calculated by the number of molecules, atomic mass, and space, is smaller than the real value. (In our case, the density of pure *n*-dodecane is 0.7511 g/cm^3 at room temperature.) Therefore, this narrowing was done until the difference of $^1/_3$ power of density become relatively small, resulting in 12% deviation for the 1-dimensional scale. The total deviation in this calculation was estimated to be 13%. Figure 6b,c is the view inside the box. For the display, the radii of the atoms were depicted smaller than the real radii. Several solvent molecules adjacent to one solute molecule were extracted and illustrated in Figure 6d.

The adjacent effect was calculated and shown in Figure 7. The solid line is the same curve as the one in Figure 5. The E_{adjacent} was obtained by varying a minimum distance between the solvent and solute molecules. We defined the minimum distance as the one between the center of solute nitrogen atom and the closest solvent atom which is the closest to the nitrogen atom. Since an unpaired electron in *n*-alkane radical cation is delocalized over the σ chain,[65,66] the solvent and solute molecules can be regarded to be adjacent if the minimum distance is less than a threshold. The closest value to the solid line was 0.5 ± 0.07 nm, which is near a typical reaction radius,[23,42,67] representing a reasonable calculation result. To

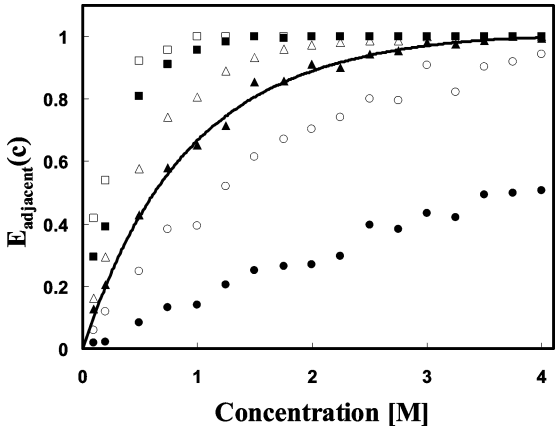

Figure 7. Adjacent effect obtained by the configurational-bias Monte Carlo simulation. The solid line is the same curve as the one in Figure 5. Each dot is the adjacent effect with various minimum distances between the solvent and solute molecules; closed circle = 0.3 nm, open circle = 0.4 nm, closed triangle = 0.5 nm, open triangle = 0.6 nm, closed square = 0.8 nm, open square = 1.0 nm. These values have an uncertainty of ±13%.

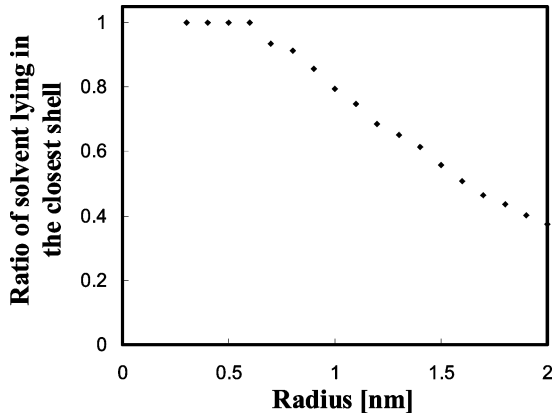

Figure 8. Relationship between a reaction radius and the ratio of solvents lying in the closest shell to other solvents which exist in the sphere. The depicted values on the horizontal axis have ±12% uncertainty.

show the validity of this threshold, we also calculated the relationship between a reaction radius and the ratio of solvents lying in the closest shell to other solvents which exist in the sphere. As seen in Figure 8, all of the solvents lies in the closest shell up to 0.6 nm, suggesting that the electron-transfer reaction occurs in the inner shell. The ratio decreases with the increase of the radius. Thus, it is confirmed that the adjacent phenomena take place between a solute and the closest shell of the solvents.

The sphere of the action model in the static quenching gives a constant radius over the whole quencher concentration, as described above. This radius which showed good agreement with the experimental data was 0.77 nm. This discrepancy of the radius between 0.5 and 0.77 nm is due to the fact that the electron delocalization of radical cation[65,66] was considered in the Monte Carlo simulation. Namely, the larger radius is overestimated because the electron delocalization of reactants is neglected. From eq 7 and the parameter set used in the calculation, we found that $V(c)$ decreased by a factor of 0.34

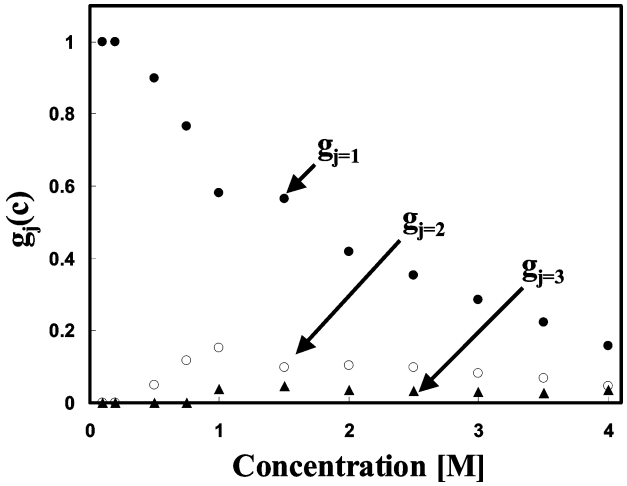

Figure 9. Distribution of the aggregating solute obtained by configurational-bias Monte Carlo simulation.

with an increase in concentration from $c = 0$ M to $c = 4$ M, giving a close radius of 0.54 nm to the one of Monte Carlo result at 4 M. When the solute concentration is large, the probability of solute that happen to exist within the 0.5 nm sphere becomes large. Therefore, The concentration-dependent radius in the sphere of action model gets close to 0.5 nm.

From the position data obtained by the Monte Carlo simulation, we determined the average number of adjacent solvent molecules which surround one target solute cluster. The obtained values are listed in Table 2. The parameter set of $b_j(c)$ used in the statistical model was $(b_1, b_2, b_3, b_4) = (5, 7, 9, 10)$, showing good correspondence.

To make a comparison of the result of Monte Carlo with the statistical model, we calculated the distribution of aggregation among solute molecules. The result is shown in Figure 9. The $j = 1$ part, which is equivalent to an isolated solute molecule, was somewhat larger than the one in Figure 3. Therefore, one finds that the curves of $j = 2$, 3 and other clusters were smaller. This is ascribed to the difference in the way we place the solute molecules. Namely, the distribution in Figure 3 was constructed randomly; thus, a certain portion of the significant overlaps between each solvent molecule was not avoided. On the other hand, the configurational-bias Monte Carlo method enables us to eliminate the overlaps.

4. Conclusion

Time-dependent behavior of radical cation in *n*-dodecane in the presence of cation scavenger TEA was measured by subpicosecond pulse radiolysis system. A significant reduction of the initial yield in the optical density was observed in the presence of TEA. This reduction was not able to be explained by the first-order rate constant and time-dependent rate coefficient. Therefore, we assumed that this phenomenon occurs due to the adjacent effect of the solute molecules.

We approached this effect using the statistical model and a configurational-bias Monte Carlo method. Both methods are based on the following assumption: the cation site in the radical cation is delocalized and will be scavenged rapidly within the

TABLE 2: Average Number of Neighboring Solvent Molecules

solute no.[a]	1	2	3	4	5	10
solvent no.[b]	4.4 ± 0.7	5.7 ± 1.3	8.0 ± 2.5	8.0 ± 2.6	9.7 ± 2.8	12.3 ± 3.3

[a] The number of solute molecules which are neighboring each other. [b] The average number of solvent molecules which are surrounding a target solute molecule.

time resolution of the measurement system if the solute molecules is adjacent to any sites of the solvent molecule In addition to the adjacent effect, the fact that a large part of the solvent molecules is excluded by the solute molecules especially at high concentration was taken into consideration.

First, we formulated this effect by a statistical model. In addition to the above assumption, this model has the following assumptions: (a) the effects of molecule's shape, conformation, and interaction among molecules were not included explicitly, and (b) the aggregation of the solute molecules were treated randomly. The formula indicated good agreement with the experimental data. We also discussed the relationship with the static quenching in the photolysis, giving the concentration-dependent V parameter.

Second, as another approach, we adopted the configurational-bias Monte Carlo simulation to reproduce the liquid system. The OPLS model was used to describe the intermolecular and intramolecular potentials. The adjacent effect estimated by this method corresponded to the experimental data with a threshold of 0.5 ± 0.07 nm. This value is close to a typical reaction radius. The relationship with the sphere of action model was discussed. Finally, the average number of adjacent solvent molecules and the distribution of aggregated solute's number were collected from the position data.

Acknowledgment. The authors thank Prof. A. D. Trifunac at Argonne National Laboratory for his helpful advice.

References and Notes

(1) Warman, J. M. *The Study of Fast Processes and Transient Species by Electron Pulse Radiolysis*; Baxendale, J. H., Busi, F., Eds.; Reidel: Dordrecht, The Netherlands, 1982.
(2) Thomas, J. K.; Johnson, K.; Klipper, T.; Lowers, R. *J. Chem. Phys.* **1968**, *48*, 1608.
(3) Sauer, M. C.; Jonah, C. D. *J. Phys. Chem.* **1980**, *84*, 2539.
(4) van den Ende, C. A. M.; Nyikos, L.; Warman, J. M.; Hummel, A. *Radiat. Phys. Chem.* **1980**, *15*, 273.
(5) Jonah, C. D. *Radiat. Phys. Chem.* **1983**, *21*, 53.
(6) Tagawa, S.; Washio, M.; Kobayashi, H.; Katsumura, Y.; Tabata, Y. *Radiat. Phys. Chem.* **1983**, *21*, 45.
(7) Tagawa, S.; Hayashi, N.; Yoshida, Y.; Washio, M.; Tabata, Y. *Radiat. Phys. Chem.* **1989**, *34*, 503.
(8) Trifunac, A. D.; Sauer, M. C.; Jonah, C. D. *Chem. Phys. Lett.* **1985**, *113*, 316.
(9) Le Motais, B. C.; Jonah, C. D. *Radiat. Phys. Chem.* **1989**, *33*, 505.
(10) Yoshida, Y.; Tagawa, S.; Washio, M.; Kobayashi, H.; Tabata, Y. *Radiat. Phys. Chem.* **1989**, *34*, 493.
(11) Yoshida, Y.; Tagawa, S. In *Dynamics and Mechanisms of Photo-induced Transfer and Related Phenomena*; Mataga, N., Okada, T., Masuhara, H., Eds.; Elsevier Science Publishers B.V.: Dordrecht, 1992.
(12) Yoshida, Y.; Ueda, T.; Kobayashi, T.; Shibata, H.; Tagawa, S. *Nucl. Instrum. Methods* **1993**, *A327*, 41.
(13) Yoshida, Y.; Tagawa, S.; Kobayashi, H.; Tabata, Y. *Radiat. Phys. Chem.* **1987**, *30*, 83.
(14) Saeki, A.; Kozawa, T.; Yoshida, Y.; Tagawa, S. *Radiat. Phys. Chem.* **2001**, *60*, 319.
(15) Saeki, A.; Kozawa, T.; Yoshida, Y.; Tagawa, S. *Jpn. J. Appl. Phys.* **2002**, *41*, 4213.
(16) Hong, K. M.; Noolandi, J. *J. Chem. Phys.* **1978**, *68*, 5163.
(17) Hong, K. M.; Noolandi, J. *J. Chem. Phys.* **1978**, *69*, 5026.
(18) Infelta, P. P.; Rzad, S. J. *J. Chem. Phys.* **1973**, *58*, 3775.
(19) Schwarz, H. A. *J. Chem. Phys.* **1971**, *55*, 3647.
(20) Magee, J. L. *J. Chem. Phys.* **1972**, *56*, 3061.
(21) Nichols, A. L.; Chandler, D. *J. Chem. Phys.* **1987**, *87*, 6671.
(22) Tachiya, M. *Radiat. Phys. Chem.* **1987**, *30*, 75.
(23) Bartczak, W. M.; Hummel, A. *J. Chem. Phys.* **1987**, *87*, 5222.
(24) Wojcik, M.; Bartczak, W. M.; Hummel, A. *J. Chem. Phys.* **1992**, *97*, 3688.
(25) Bronskill, M. J.; Taylor, W. B.; Wolff, R. K.; Hunt, J. W. *Rev. Sci. Instrum.* **1970**, *41*, 333.
(26) Jonah, C. D. *Rev. Sci. Instrum.* **1975**, *46*, 62.
(27) Kobayashi, H.; Tabata, Y. *Nucl. Instrum. Methods* **1985**, *B10/11*, 1004.
(28) Yoshida, Y.; Ueda, T.; Kobayashi, T.; Tagawa, S. *J. Photopolym. Sci. Technol.* **1991**, *4*, 171.
(29) Wishart, J. F. *Stud. Phys. Theor. Chem.* **2001**, *87*, 21.
(30) Muroya, Y.; Lin, M.; Watanabe, T.; Wu, G.; Kobayashi, T.; Yoshii, K.; Ueda, T.; Uesaka, M.; Katsumura, Y. *Nucl. Instrum. Methods* **2002**, *A489*, 554.
(31) Kozawa, T.; Mizutani, Y.; Yokoyama, K.; Okuda, S.; Yoshida, Y.; Tagawa, S. *Nucl. Instrum. Methods* **1999**, *A429*, 471.
(32) Kozawa, T.; Mizutani, Y.; Miki, M.; Yamamoto, T.; Suemine, S.; Yoshida, Y.; Tagawa, S. *Nucl. Instrum. Methods* **2000**, *A440*, 251.
(33) Bartels, D. M.; Cook, A. R.; Mudaliar, M.; Jonah, C. D. *J. Phys. Chem. A* **2000**, *104*, 1686.
(34) Kozawa, T.; Saeki, A.; Yoshida, Y.; Tagawa, S. *Jpn. J. Appl. Phys.* **2002**, *41*, 4208.
(35) Wolff, R. K.; Bronskill, M. J.; Hunt, J. W. *J. Chem. Phys.* **1970**, *53*, 4211.
(36) Lam, K. Y.; Hunt, J. W. *Int. J. Radiat. Phys. Chem.* **1975**, *7*, 317.
(37) Thomas, J. K.; Gordon, S.; Hart, E. J. *J. Phys. Chem.* **1964**, *68*, 1524.
(38) Domae, M.; Katsumura, Y.; Jiang, P. Y.; Nagaishi, R.; Ishigure, K.; Kozawa, T.; Yoshida, Y. *J. Chem. Soc., Faraday Trans.* **1996**, *92*, 2245.
(39) Czapski, G.; Peled, E. *J. Phys. Chem.* **1973**, *77*, 893.
(40) Bühler, R. E.; Katsumura, Y. *J. Phys. Chem. A* **1998**, *102*, 111.
(41) de Haas, M. P.; Warman, J. W.; Infelta, P. P.; Hummel, A. *Chem. Phys. Lett.* **1975**, *31*, 382.
(42) Warman, J. W.; Infelta, P. P.; de Haas, M. P.; Hummel, A. *Chem. Phys. Lett.* **1976**, *43*, 321.
(43) Sauer, M. C.; Trifunac, A. D.; McDonald, D. B.; Cooper, R. *J. Phys. Chem.* **1984**, *88*, 4096.
(44) Trifunac, A. D.; Sauer, M. C.; Jonah, C. D. *Chem. Phys. Lett.* **1985**, *113*, 316.
(45) Shkrob, I. A.; Liu, A. D.; Sauer, M. C.; Schmidt, K. H.; Trifunac, A. D. *J. Phys. Chem. B* **1998**, *102*, 3371.
(46) Sauer, M. C.; Shkrob, I. A.; Yan, J.; Schmidt, K. H.; Trifunac, A. D. *J. Phys. Chem.* **1996**, *100*, 11325.
(47) Shkrob, I. A.; Sauer, M. C.; Trifunac, A. D. *J. Phys. Chem.* **1996**, *100*, 7237.
(48) To estimate the exclusive volume ratio of TEA in *n*-dodecane solution, weights of each molecule in the graduated flask were measured, and the ratio was calculated by $(w_{dod}/M_{dod} - w^{mix}{}_{dod}/M_{dod})/(w^{mix}{}_{TEA}/M_{TEA})$, where M_{dod}, M_{TEA}, w_{dod}, $w^{mix}{}_{dod}$, and $w^{mix}{}_{TEA}$ are the molecular weight of *n*-dodecane, molecular weight of TEA, weight of *n*-dodecane in the graduated flask filled by only *n*-dodecane, and weights of *n*-dodecane and TEA in the same volume graduated flask filled by *n*-dodecane and TEA mixture, respectively.
(49) Frank, I. M.; Vavilov, S. I. *Z. Phys. Chem. (Munich)* **1931**, *69*, 100.
(50) Eftink, M. R.; Ghiron, C. A. *J. Phys. Chem.* **1976**, *80*, 486.
(51) Wang, J.; Wang, D.; Miller, E. K.; Moses, D.; Bazan, G. C.; Heeger, A. J. *Macromolecules* **2000**, *33*, 5153.
(52) Weller, A. *Prog. React. Kinet.* **1961**, *1*, 187.
(53) Boaz, H.; Rollefson, G. K. *J. Am. Chem. Soc.* **1950**, *72*, 3435.
(54) Shida, T. *Electronic Absorption Spectra of Radical Ions*; Elsevier: New York, 1988.
(55) Mooiji, G. C. A. M.; Frenkel, D.; Smit, B. *J. Phys.: Condens. Matter* **1992**, *4*, L255.
(56) Lao, M.; de Pablo, J. J.; Suter, U. W. *J. Chem. Phys.* **1992**, *97*, 2817.
(57) de Pablo, J. J.; Bonnin, M.; Prausnitz, J. M. *Fluid Phase Equilib.* **1992**, *73*, 187.
(58) Smit, B.; Karaborni, S.; Siepmann, J. I. *J. Chem. Phys.* **1995**, *102*, 2126. Smit, B.; Karaborni, S.; Siepmann, J. I. *J. Chem. Phys.* **1998**, *109*, 35.
(59) Jorgensen, W. L.; Madura, J. D.; Swenson, C. J. *J. Am. Chem. Soc.* **1984**, *106*, 6638.
(60) Hautman, J.; Klein, M. L. *J. Chem. Phys.* **1989**, *91*, 4994.
(61) Rizzo, R. C.; Jorgensen, W. L. *J. Am. Chem. Soc.* **1999**, *121*, 4827.
(62) Jorgensen, W. L.; Maxwell, D. S.; Tirado-Rives, J. *J. Am. Chem. Soc.* **1996**, *118*, 11225.
(63) Van der Ploeg, P.; Berendsen, H. J. C. *J. Chem. Phys.* **1982**, *76*, 3271.
(64) Ryckaert, J. P.; Bellemans, A. *Chem. Phys. Lett.* **1975**, *30*, 123.
(65) Toriyama, K.; Nunome, K.; Iwasaki, M. *J. Phys. Chem.* **1986**, *90*, 6836.
(66) Toriyama, K.; Nunome, K.; Iwasaki, M. *J. Phys. Chem.* **1981**, *85*, 2149.
(67) Lefkowitz, S. M.; Trifunac, A. D. *J. Phys. Chem.* **1984**, *88*, 77.